

# On Systematic Errors of Two-Dimensional Finite Element Modeling of Right Circular Planar Flexure Hinges

B. Zettl

W. Szyszkowski

W. J. Zhang

Department of Mechanical Engineering,  
University of Saskatchewan,  
Saskatoon, S7N A9V, Canada

*This paper discusses the finite element method (FEM) based modeling of the behavior of typical right circular flexure hinges used in planar compliant mechanisms. Such hinges have traditionally been approximated either by simple beams in the analytical approach or very often by two-dimensional (2D) plane stress elements when using the FEM. The three-dimensional (3D) analysis presented examines these approximations, focusing on systematic errors due to 2D modeling. It is shown that the 2D models provide only the lower (assuming the plane stress state) or the upper (assuming the plane strain state) limits of the hinge's stiffness. The error of modeling a particular hinge by 2D elements (with either the plane stress or the plane strain assumptions) depends mainly on its depth-to-height ratio and may reach up to about 12%. However, this error becomes negligible for hinges with sufficiently high or sufficiently low depth-to-height ratios, in which either the plane strain or stress states dominate respectively. It is also shown that the computationally intensive 3D elements can be replaced, without sacrificing accuracy, by numerically efficient 2D elements if the material properties are appropriately manipulated. [DOI: 10.1115/1.1898341]*

## 1 Introduction

Compliant mechanisms are almost universally used in modern micropositioning systems and microelectromechanical systems devices to transform a given input to some useful or meaningful output. Such mechanisms, unlike conventional mechanisms, are monolithic structures that provide the required motion by way of flexible elements inherent in the structure.

One common flexible element for revolute type motion is the flexure hinge. This paper focuses on the right-circular planar flexure hinge; however, the modeling problems discussed here will most probably be similar for planar flexure hinges of any profile. Typically, the hinges are placed between relatively rigid elements, referred to as links, to provide a planar motion of the mechanism's members. Since the motion is planar, it may be tempting to assume that all aspects of the mechanism's behavior are so, including the stress-strain states in the hinges; however, it will be demonstrated in the paper that this is not entirely correct.

In order to reduce any parasitic out-of-plane motion and to make the mechanism as flexible as possible the modern hinges often have high depth-to-height ratios, in the paper referred to as the  $b/t$  ratio (see Fig. 1). Although the stress distribution due to bending in such hinges does not follow the plane stress assumptions, the finite element method (FEM) simulations of the planar flexure hinge's behavior, as published in the relevant literature, has been done almost exclusively using 2D plane stress elements. Clearly, any such 2D analysis produces a systematic modeling error, which is dependent upon the particular hinge dimensions and may be significant. The earlier modeling issues are discussed in detail in this paper.

The early works on flexible hinges used analytical methods and approximated the hinge simply as a beam in bending. For example, the classical Euler-Bernoulli beam equation was used in Ref. [1] to determine the hinge compliance. In spite of a rather

rudimentary character of such a model, the formulas derived in this work are still used to provide a preliminary prediction of the hinge behavior [2,3]. Such an approach can be considered as a one-dimensional (1D) approximation of the hinge mechanics, since only one stress component is accounted for in the beam model.

A more realistic modeling of the hinge is possible using the FEM approach. However, despite a recent development in the FEM software a full three-dimensional (3D) analysis, which could produce the most accurate results, is still considered too intensive numerically and somewhat impractical. On the other hand, the 3D analysis seems to have been judged unnecessary, most probably due to the planar character of the hinge motion. Instead, a much simpler two-dimensional (2D) modeling strategy has been used throughout [4–8]. Clearly, the 2D models neglect any stress/strain variation across the hinge's depth. Two options are easily available in 2D modeling, namely the plane stress state or the plane strain state, in which either the stress components or the strain components in the depth direction are neglected, respectively. Although not always explicitly stated, virtually all the papers mentioned earlier seemed to have assumed the plane stress state. Moreover, experimental results were often compared to the 2D computer models, in which the planar geometry was preserved, but the depth-to-height ratio of the hinge was not. For example, in Ref. [5] the hinge of a  $b/t$  ratio equal to 10 was analyzed by the FEM. However, the laboratory model for experimental verifications was fabricated with a  $b/t$  ratio of only 2.2. As it will be shown later in the paper, despite their identical planar profiles such hinges are not similar (the plane strain state dominates the behavior of the hinge if  $b/t=10$ , while the plane stress state dominates the behaviour of the hinge if  $b/t=2.2$ ). Exceptions to the above 2D analyses are the works in Refs. [9,10] where 3D elements were used. However, the mesh used in Ref. [9] to model a notched planar hinge appears to be coarse, and not enough details were reported to evaluate accuracy of the model. No details of the FEM modeling of the entire compliant mechanism in Ref. [10] was provided.

As already mentioned, the plane stress state assumption is ques-

Contributed by the Mechanisms and Robotics Committee for publication in the JOURNAL OF MECHANICAL DESIGN. Manuscript received April 22, 2004; revised September 17, 2004. Associate Editor: G. K. Ananthasuresh.

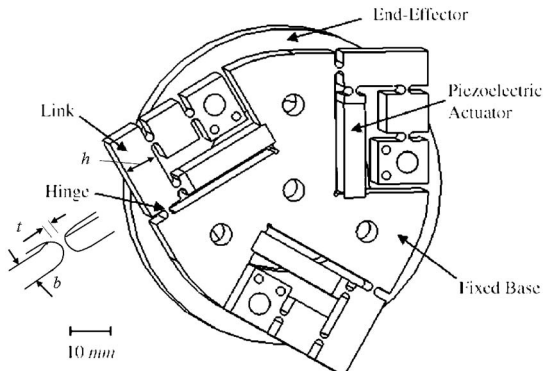


Fig. 1 Piezoactuated compliant mechanism

tionable for most of the planar hinges presently used. Moreover, due to a high  $b/t$  ratio and a large stiffness of adjacent links, it is the strain in the depth directions (not the stress) that appears to be negligible in large portion of the hinge. Consequently, one should rather expect a better 2D approximation if applying the plane strain elements, than if applying the plane stress elements.

This paper presents a 3D analysis of a right-circular hinge. Several symmetry/antisymmetry planes are used to reduce the number of degrees of freedom (DOF). Despite this, the model developed may still be considered computationally intensive and it might be too difficult to use it for the dynamic analyses or optimization of the whole compliant mechanism. However, the model permits one to verify the assumptions used in 2D models, and to determine how the accuracy of 2D modeling with either the plane strain or plane stress elements is affected by the  $b/t$  ratio.

## 2 Flexure Hinges

A typical piezoactuated compliant mechanism used as a micro-positioning system is shown in Fig. 1. It consists of the actuators, several links connected by flexible hinges, and the end-effector that can move in the  $x$ - $y$  plane.

The FEM analysis presented here is done for a single hinge shown in Fig. 2. Planar mechanisms are usually cut from a plate

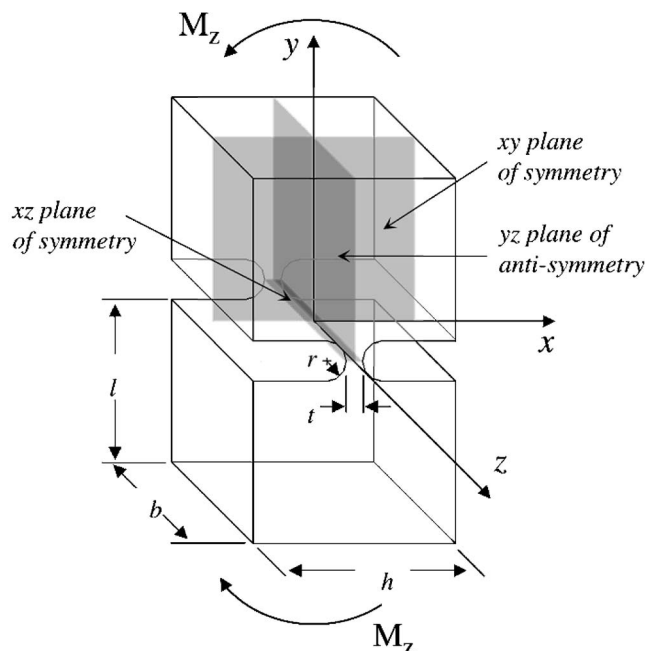


Fig. 2 Right circular hinge used in finite element study

Table 1 Parameters of the flexure hinge model

Hinge Parameter	Value (mm)
$b$	10
$h$	10
$l$	8
$r$	1
$t$	0.8

of uniform thickness, denoted here by  $b$ . In terms of the hinge geometry, the dimensions  $b$  and  $t$  will be referred to as the depth and height, respectively. For the hinges in Fig. 1 the  $b/t$  ratio is 12.5. The height of the hinge,  $t$ , is typically much smaller than the height of the link  $h$  (for example, for this particular mechanism the ratio  $t/h$  is 0.08). The bending stiffness ratio of these two members is approximately equal to  $(t/h)^3$  and is very small in practice. Therefore, the deformability of links is often negligible, and they are considered to be rigid members [11]. The numerical values assigned to the parameters of the hinge are given in Table 1.

In the FEM model, the hinge's geometry is recreated "exactly;" however, only a small portion of the link is included, denoted here by  $l$ . The value of  $l$  is selected such that the effects of the hinge geometry on the stress distribution in the links become negligible. The height of the link  $h$  is assumed identical for both adjacent links, which is justified by the numerical experimentations indicating that the  $h$  value becomes irrelevant for the  $t/h$  ratio smaller than about 0.25.

Flexure hinges are inherently designed to bend. In order to investigate their behavior in bending the model of the hinge is loaded with a moment  $M_z$  at either end of the hinge. The material behavior is assumed linearly elastic, isotropic, and homogeneous. The Young's modulus of  $E=105$  GPa, and a Poisson ratio of  $\mu=0.33$  are used.

The origin of the coordinate system is positioned at the centre of the hinge with the  $z$  axis representing the depth. As indicated in Fig. 2, the model has two planes of symmetry ( $xy$  and  $xz$ ) and one plane of antisymmetry ( $yz$ ). These planes will be used to reduce the number of DOF of the FEM analysis, as only one eighth of the hinge needs to be modeled.

## 3 Finite Element Models

The reference model of this study is a 3D model (see Fig. 3)

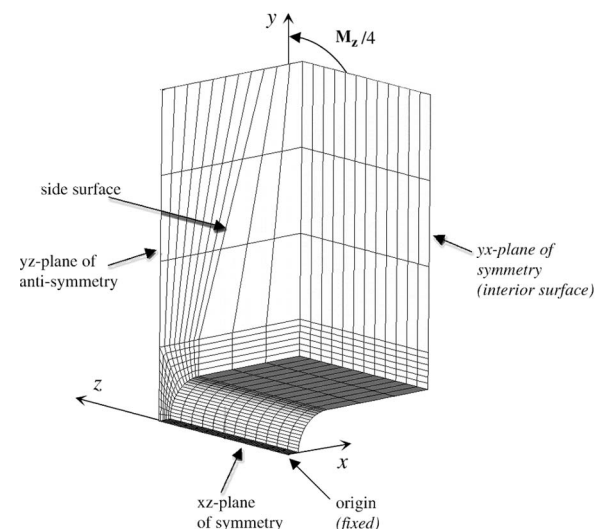


Fig. 3 3D finite element hinge model

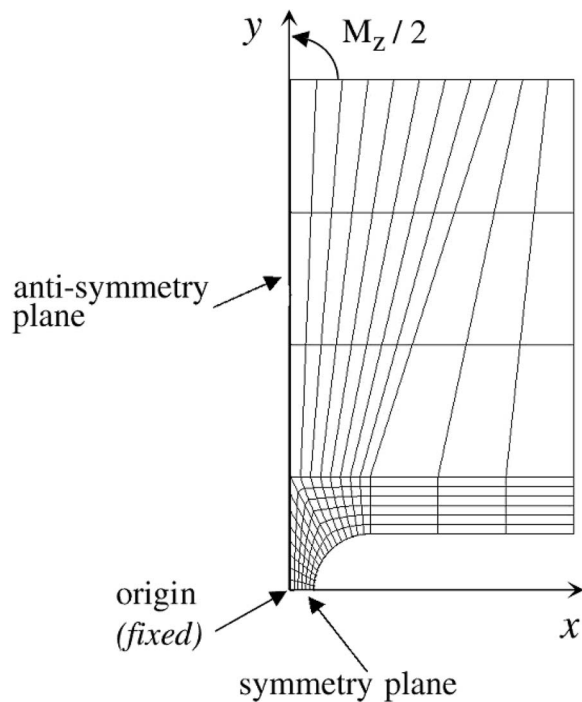


Fig. 4 2D finite element model of hinge

meshed with 20-node brick elements, SOLID95, available from the ANSYS software. These elements use quadratic shape functions to approximate displacements. Each side of the element has eight nodes, and complex geometries can be modeled with high fidelity due to midside nodes. As already mentioned the model employs two planes of symmetry ( $xy$  and  $xz$ ) and one plane of antisymmetry ( $yz$ ).

Since the brick elements do not have rotational DOFs, the bending moment was applied, for convenience, via several fictitious beam elements attached to the top-most  $x$ - $z$  face of the model. These beam elements are sized such that their bending stiffness approaches infinity, but their axial stiffness is close to zero so that the plane  $y=r+l$  remains flat when a given moment is applied. For  $l \geq 8$  mm the model generates linearly distributed stresses  $\sigma_y$  at the link's end.

The 3D model was coded in a parametric fashion and meshed to secure convergence. The meshing becomes coarser in the link portion, because the stress/strain field developed in this portion is almost constant and relatively small. The model shown in Fig. 3 has approximately 24,000 active DOFs. It should be emphasized that using more elements (and more DOFs) in this model is not affecting the displacement and stress results.

The corresponding 2D model, which is a planar representation of the  $x$ - $y$  face of the 3D model, is shown in Fig. 4. The eight-node quadrilateral elements, PLANE82, are used with the option of using either a plane stress or plane strain stress state. These elements can be considered as 2D equivalent of the 20-node brick elements used in the 3D model.

The model was constrained in the same way as the 3D model. The bending moment was applied via fictitious beam elements at the model similarly as before. This model has approximately 1000 active DOF. It has also been tested for convergence by examining the sensitivity of displacements and stresses to particular meshing.

#### 4 Stress/Strain Results of 3D Model

The stress/strain states of the 3D model along the edges  $AB$ ,  $OA$ , and  $CB$  indicated in Fig. 5 will be discussed first. The hinge's view in Fig. 5 is the same as in Fig. 3. Note that path  $CB$  is on the

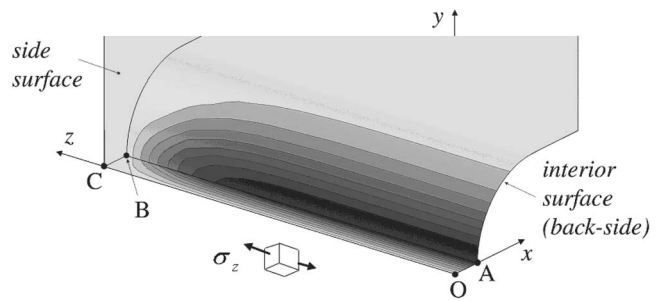


Fig. 5 Contours of stress  $\sigma_z$  from no-stress (light) to high-stress (dark)

free side surface of the hinge ( $z=0.5b$ ), while path  $OA$  is located on the symmetry plane at the center ( $z=0$ ). The bending moment of 200 N mm is applied. The contours of the nodal stress in the  $z$  direction ( $\sigma_z$ ) are shown, the darker the color the higher the stresses with the maximum value reaching 65.8 MPa. The bright area essentially indicates the plane stress state with negligibly small stress  $\sigma_z$ , while the dark area indicates the plane strain state with negligibly small strain  $\epsilon_z$ , as explained later in this section. The maximum stress in the  $y$ -direction was  $\sigma_y=219.3$  MPa. If the hinge were modeled as a beam, the maximum value of this stress component would be 187.5 MPa (neglecting any stress concentration). Only the tensioned quarter of the hinge is analyzed. The stress and strain components for path  $AB$  are plotted in Fig. 6(a) and 6(b), respectively.

It becomes immediately apparent that on the side surface, at point  $B$  ( $z=5$  mm), the stress  $\sigma_z=0$ , and also  $\epsilon_z=-\mu\epsilon_y$ , which indicates the plane stress state. However, the plane stress conditions disappear quickly when moving away from the side surface.

On the other hand, at the center of the hinge (at point  $A$ , or  $z=0$ ), the strains  $\epsilon_z=0$ ,  $\epsilon_x=-\mu\epsilon_y$ , and also  $\sigma_z=\mu\sigma_y$ , which represents the plane strain state conditions. The plane strain conditions are preserved roughly up to about 4 mm, i.e., for about 80% of the bent section.

The stress  $\sigma_y$  along paths  $OA$  and  $BC$  are plotted in Fig. 7. For comparison, the stress distribution according to the beam theory (which corresponds to the Paros-Weisberg model in Ref. [1]) is also indicated.

The deformation pattern is presented in Fig. 8. The lateral displacement,  $v_x(y)$ , due to bending of the hinge along the plane of antisymmetry is plotted in Fig. 8. This plot shows that the slope of the deflected link (for  $y \geq r=1$  mm) is essentially constant. Therefore, for any practical purposes, the slope  $\alpha$  and the deflections  $v_x$  calculated at  $y=r$  can be considered as representative for the hinge flexibility.

Further confirmation of a mixture of the plane stress and plane strain states in the hinge can be found by examining the deformation pattern of the  $x$ - $z$  plane of the hinge center. A graphical representation of the deformation is presented in Fig. 9 that depicts the full  $x$ - $z$  plane of the hinge center. A displacement-scaling factor of 500 was used.

Along  $B'B'$  ( $\approx 80\%$  of the cross section) the deformation is characteristic of the plane strain state. The strain  $\epsilon_z$  in this section is almost completely constrained. Only close to the side surfaces at points  $B$  does the deformation become characteristic of the plane stress state. Thus for this particular geometry the plane strain states dominates the hinge behavior.

#### 5 Comparison of 3D Models with 2D Models

The 2D approximations of the hinge was analyzed assuming either the plane stress or the plane strain states for the FEM model in Fig. 4. For both states the contours of stress  $\sigma_y$  are the same as in the 3D model; however, the maximum stress reduces slightly to

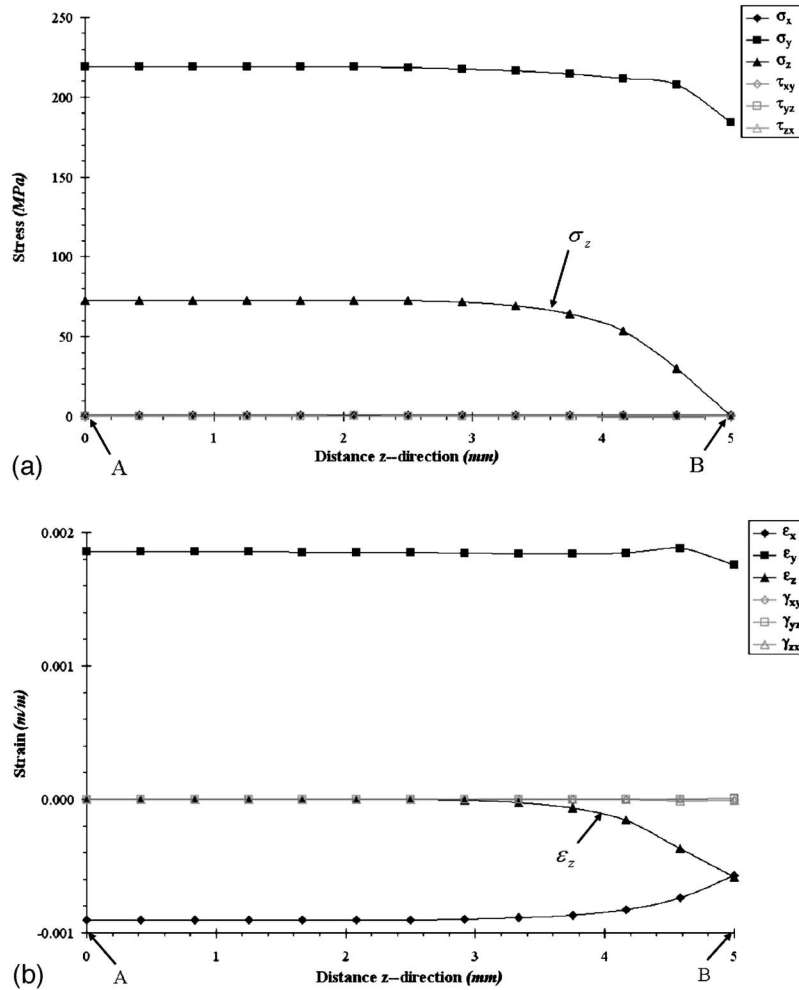


Fig. 6 (a) Stresses along path AB. (b) Strains along path AB.

215 MPa. The lateral deflection pattern is also similar to that shown in Fig. 8, but the values of the rotation angle  $\alpha$  and the displacement  $v_x$  are different. These values reflect the stiffness characteristics of the hinge that are the most important parameters required for accurate modeling of compliant mechanisms. Since the link essentially rotates as a rigid body the hinge's flexibility can be characterized by the slope  $\alpha$  and deflection  $v_x$ , which for a given bending moment  $M_z$  can be obtained either from the 3D model or from the 2D approximations. The stiffnesses of the hinge are defined by

$$k_\alpha = \frac{M_z}{\alpha} \quad (1)$$

$$k_v = \frac{M_z}{v_x} \quad (2)$$

The FEM results are also compared with the beam approximation referred to as the Paros-Weisbord stiffness formulas [1], according to which

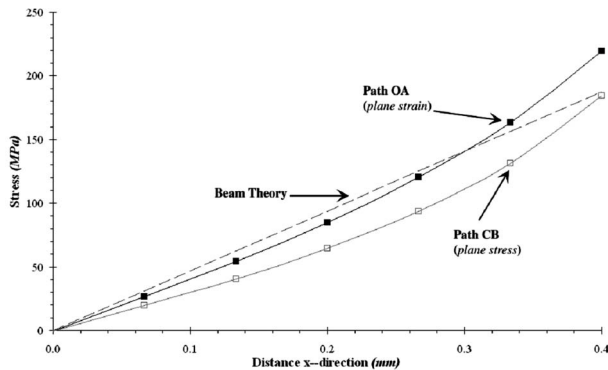


Fig. 7 Stress in y direction along path OA and BC

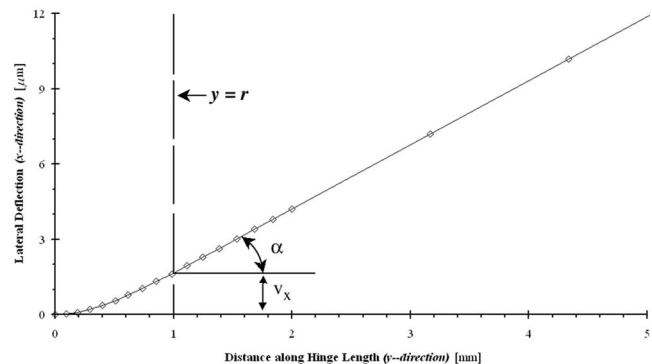


Fig. 8 Deflection along hinge length

**Table 2 Rotational and lateral bending stiffnesses obtained from various models**

Model	$k_\alpha$ (Nm/rad)	$k_\nu$ (kN m/m)
3D	78.23	120.1
2D plane strain	79.68 (+1.9%)	122.2 (+1.7%)
2D plane stress	71.00 (-9.2%)	110.5 (-8.0%)
1D beam	85.0 (+8.7%)	85.0 (-29.2%)

$$k_\alpha = \frac{4Ebt^{5/2}}{9\pi r^{1/2}} \quad (2a)$$

$$k_\nu = \frac{k_\alpha}{r} \quad (2b)$$

These formulas represent a 1D approximation of the hinge behavior. The second formula assumes that  $\nu_x \cong \alpha \cdot r$ . Note, however, that  $\nu_x = 1.665 \mu\text{m}$  and  $\alpha \cdot r = 2.556 \mu\text{m}$  (about 53% difference) according to the results presented in Fig. 8, which indicates a rather poor accuracy of the above assumption.

The stiffnesses  $k_\alpha$  and  $k_\nu$  obtained from various models are listed in Table 2. The values calculated from the 3D model (78.23 and 120.1, respectively) are considered to be the most accurate. The stiffness calculated from the 2D model with the plane strain assumption (79.68 and 122.2, respectively) are slightly overestimated. This should be expected since the plane strain model would be almost exact for about 80% of the hinge's bent section. On the other hand, the 2D model with the plane stress assumption underestimates the stiffnesses (71.00 and 110.5, respectively) by some 8–9%. This is because only less than 20% of the hinge's section appears to meet the plane stress conditions.

It should be noted that the ratio of stiffness of a bent member obtained from the plane strain and plane stress should theoretically be equal to  $(1-\mu^2)^{-1}$ . In our case this ratio is 1.122 (for Poisson's ratio of 0.33) that agrees very well with the theoretical prediction. The real stiffness must always be between those obtained from 2D models with either the plane strain state (overestimation) or the plane stress state (underestimation). Therefore, it can be concluded that, in general, the error of 2D modeling of the hinge should not exceed about 12%. The 1D approximations from (2a) and (2b) are somewhat inconsistent in a sense that the rotational stiffness is overestimated by 8.7%, while the lateral stiffness is underestimated by 29.2%.

## 6 Classification of Hinges

The results presented in Table 2 were obtained for the hinge of the  $b/t$  ratio equal to 12.5. Clearly, the hinge of such proportions is better represented by the plane strain elements than by the plane stress elements in a 2D analysis. In order to understand the effects of the depth-to-height ratio on the hinge's behavior the complete 3D analyses have been repeated for the depth  $b$  varied incrementally from 0.2 to 20 mm, and the  $b/t$  ratio changing from 0.25 to 25, respectively. The results for the stiffness per unit of the depth, to be referred to as the specific stiffness, are presented in Fig. 10. The specific stiffnesses obtained from the 3D model are indicated by the superscript "3D" (i.e.,  $k_\alpha^{3D} = k_\alpha/b$  and  $k_\nu^{3D} = k_\nu/b$ ), while the specific stiffnesses obtained from the 2D model by either the su-

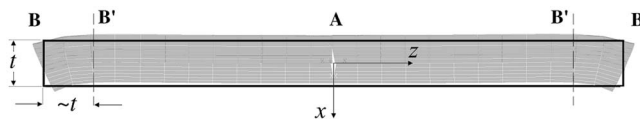


**Fig. 9 Deformation of the xz-plane hinge center during bending**

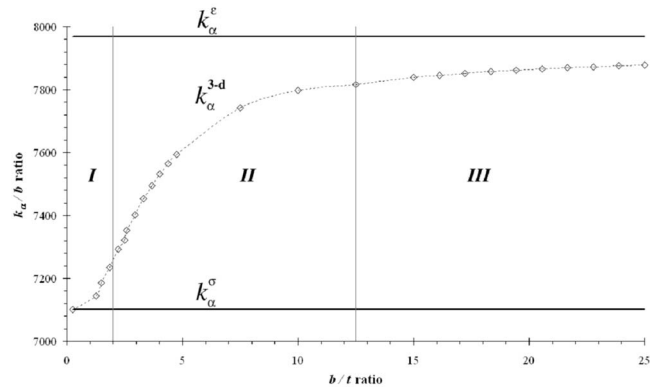


**Fig. 10 Rotational stiffness as a function of  $b/t$  ratio**

perscript "σ" ( $k_\alpha^\sigma$  and  $k_\nu^\sigma$ ) for the plane stress state or "ε" ( $k_\alpha^\epsilon$  and  $k_\nu^\epsilon$ ) for the plane strain state. Note that the specific stiffnesses of the 2D models are independent of the depth  $b$ . The specific stiffness  $k_\alpha^{3D}$  increases with the increasing depth-to-height ratios. As expected the values of  $k_\alpha^{3D}$  are bound between the stiffnesses obtained from the plane stress and plane strain states. This stiffness is approaching  $k_\alpha^\sigma$  (for the plane stress) in the domain labeled I, and  $k_\alpha^\epsilon$  (for the plane strain) in domain III.

The domains I, II, and III were selected by examining relative errors  $\Delta k_\alpha^\epsilon$  and  $\Delta k_\alpha^\sigma$  resulting from either the plane strain or plane stress state assumptions in the 2D analyses. These errors are defined as

$$\Delta k_\alpha^\epsilon = 100 \frac{k_\alpha^\epsilon - k_\alpha^{3D}}{k_\alpha^{3D}} \quad (3)$$

$$\Delta k_\alpha^\sigma = 100 \frac{k_\alpha^{3D} - k_\alpha^\sigma}{k_\alpha^{3D}} \quad (4)$$

The above errors are plotted in Fig. 11 in terms of the  $b/t$  ratio. It should be noted that the error  $\Delta k_\alpha^\sigma$  is less than 2% if  $b/t < 2$ , and the error  $\Delta k_\alpha^\epsilon$  is less than 2% if  $b/t > 12.5$ .

Almost identical results were obtained for the lateral stiffness  $k_\nu$ . The limits of domains I and III were defined using the above threshold of 2% of acceptable error.

If a hinge falls into domain I, it can be analysed with less than 2% error by using 2D plane stress elements. Such a hinge may be classified as "thin." On the other hand, if a hinge falls into domain III, it can be analyzed using a 2D model assuming the plane strain state and may be classified as "thick."

Any hinge that is neither thin nor thick falls into domain II (for  $2 \leq b/t \leq 12.5$ ) and should be analyzed by 3D models. However, the results of such analyses can be utilized to build equivalently

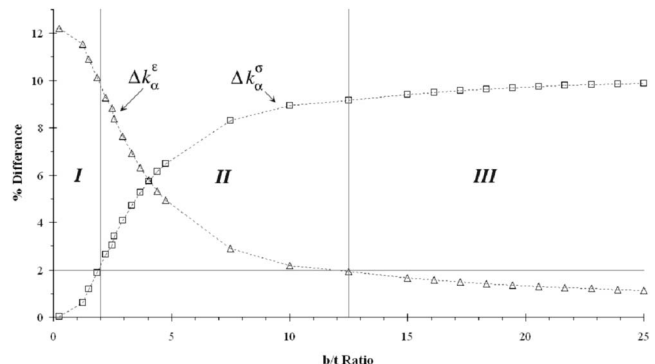


**Fig. 11 Percent errors of plane states as a function of  $b/t$  ratio**

accurate 2D models, which may be useful for other purposes. Since the hinge stiffness and its elastic modulus are proportional, one can assume that the ratio  $k_{\alpha}^{3D}/k_{\alpha}^{\sigma}$  (which can be read from Fig. 10) also represents the modification to the modulus that would be required if the 2D model with the plane stress assumption were used. The “effective” Young modulus of such a model should be calculated from

$$E_{\text{eff}} = E \frac{k_{\alpha}^{3D}}{k_{\alpha}^{\sigma}} \quad (5)$$

For example, for the hinge considered in Sec. 4 (with  $b/t=12.5$ ), for which  $k_{\alpha}^{3D}=7823$  N/rad,  $k_{\nu}^{3D}=1.201 \cdot 10^7$  N/m, and  $k_{\alpha}^{\sigma}=7100$  N/rad, the effective Young modulus becomes  $E_{\text{eff}}=115.7$  GPa. Using this modulus in the 2D plane stress model yields  $\hat{k}_{\alpha}^{\sigma}=7823$  N/rad and  $\hat{k}_{\nu}^{\sigma}=1.202 \cdot 10^7$  N/m (the hat indicates the use of effective Young modulus in the FEM simulation) reproducing very accurately the stiffnesses obtained from the 3D model.

The 2D model (with  $E_{\text{eff}}$  instead of  $E$ ) is computationally much more efficient than the 3D model, mainly due to a significantly reduced number of DOFs (from 24,000 to 1000 in our case), which may be particularly beneficial when attempting more computationally demanding analyses such as simulation of the transient dynamics or optimization of the whole compliant mechanism.

The strategy outlined above can obviously be used for planar hinges of any other profiles. For such a hinge a separate 3D model, similar to that shown in Fig. 3, would be required to obtain  $k_{\alpha}^{3D}$  and then the corresponding  $E_{\text{eff}}$ , which in turn could be applied in a 2D model of the hinge to be incorporated into the FEM model of the whole mechanism.

The results presented in Fig. 10 (or in Fig. 11) can be used to approximate the  $k_{\alpha}^{3D}/k_{\alpha}^{\sigma}$  ratio for the right circular hinges in terms of the depth-to-height ratio. For example, the following simple formula derived by interpolating the numerical data in Fig. 10 may be adopted:

$$\frac{E_{\text{eff}}}{E} = \frac{k_{\alpha}^{3D}}{k_{\alpha}^{\sigma}} \cong \frac{1}{1 - \frac{\mu^2}{1 + 11.2 \left(\frac{t}{b}\right)^{1.75}}} \quad (6)$$

Note that the plane stress case is obtained if  $b/t \rightarrow 0$ , and the plane strain case if  $b/t \rightarrow \infty$ . Also, a 2% error threshold (which corresponds to the values of  $k_{\alpha}^{3D}/k_{\alpha}^{\sigma}$  equal to 1.020 and 1.101, respectively) for  $b/t=2$  and  $b/t=12.5$  is closely recovered.

In order to illustrate the accuracy of Eq. (6) a hinge with a  $b/t$  ratio of 4.75 was analyzed. The specific stiffnesses of this hinge are:  $k_{\alpha}^{3D}=7611$  N/rad and  $k_{\nu}^{3D}=1.175 \cdot 10^7$  N/m, as determined from the 3D model. Running the 2D plane stress model without the Young’s modulus modification resulted in:  $k_{\alpha}^{\sigma}=7100$  N/rad and  $k_{\nu}^{\sigma}=1.105 \cdot 10^7$  N/m, rendering systematic errors of  $-6.7\%$  and  $-6.0\%$ , respectively. In order to improve the accuracy of the above 2D model the Young’s modulus, using Eq. (6), was shifted

from  $E=105$  GPa to  $E_{\text{eff}}=112.0$  GPa ( $E_{\text{eff}}$  would be equal to 112.6 GPa, if Eq. (5) were applied). The new 2D plane stress analysis (with  $E_{\text{eff}}$  instead of  $E$ ) yielded:  $\hat{k}_{\alpha}^{\sigma}=7571$  N/rad and  $\hat{k}_{\nu}^{\sigma}=1.170 \cdot 10^7$  N/m. The difference between these results and the values obtained from the 3D analysis is only  $-0.53\%$  and  $-0.48\%$ , respectively.

## 7 Conclusion

The stress-strain behavior of typical planar flexure hinges is affected by the adjacent rigid links and is 3D in nature. As such it should be modeled by 3D elements in order to obtain accurate predictions from the FEM simulations. Furthermore, the 3D analysis presented in the paper reveals that the plane strain conditions prevail in a significant portion of typical modern hinges, while the plane stress state is followed only in a small zone near the free surfaces. It makes the usual application of 2D plane stress elements to simulate such hinges somewhat questionable.

On the other hand, a 2D analysis (which requires significantly less numerical effort) should be acceptable for hinges that are either thin (if  $b/t < 2$ , for the right circular hinge) or thick (if  $b/t > 12.5$ , for the right circular hinge), but only if the thin hinges are modeled by the plane stress elements, and the thick hinges are modeled by the plane strain elements.

Hinges that are neither thin nor thick necessitate full 3D modeling. However, the 3D model of the hinge can be eliminated from further analyses by replacing it with the equivalently accurate but much more numerically efficient 2D models, in which the Young modulus of the material is properly modified. Such an approach might be convenient for the FEM analysis and simulation of entire compliance mechanisms.

## References

- [1] Paros, J. M., and Weisbord, L., 1965, “How to Design Flexure Hinges,” *Mach. Des.*, **37**, pp. 151–156.
- [2] Rong, Y., Zhu, Y., Luo, Z., and Liu, X., 1994, “Design and Analysis of Flexure-Hinge Mechanism Used in Micro-Positioning Stage,” *ASME J. Manuf. Sci. Eng.*, **68-2**, pp. 979–986.
- [3] Ryu, J. W., Gweon, D.-G., and Moon, K. S., 1997, “Optimal Design of a Flexure Hinge Based XY  $\theta$  Wafer Stage,” *Precis. Eng.*, **21**, pp. 18–28.
- [4] Her, I., and Chang, J. C., 1994, “A Linear Scheme for the Displacement of Micropositioning Stages with Flexure Hinges,” *ASME J. Mech. Des.*, **116**, pp. 770–776.
- [5] Lobontiu, N., Paine, J. S. N., Garcia, E., and Goldfarb, M., 2001, “Corner-Filletted Flexure Hinges,” *ASME J. Mech. Des.*, **123**, pp. 346–352.
- [6] Ragulskis, K. M., Arutunian, M. G., Kochikian, A. V., and Pogossain, M. Z., 1989, “A Study of Fillet Type Flexure Hinges and Their Optimal Design,” *Vibration Engineering*, **3**, pp. 447–452.
- [7] Smith, S. T., Badami, V. G., Dale, J. S., and Xu, Y., 1997, “Elliptical Flexure Hinges,” *Rev. Sci. Instrum.*, **68(3)**, pp. 1474–1483.
- [8] Xu, W., and King, T., 1996, “Flexure Hinges for Piezoactuator Displacement Amplifiers: Flexibility, Accuracy, and Stress Considerations,” *Precis. Eng.*, **19**, pp. 4–10.
- [9] Zhang, S., and Fasse, E. D., 2001, “A Finite-Element-Based Method to Determine the Spatial Stiffness Properties of a Notch Hinge,” *ASME J. Mech. Des.*, **123**, pp. 141–147.
- [10] Mankame, N. D., and Ananthasuresh, G. K., 2004, “A Novel Compliant Mechanism for Converting Translation into Enclosing Curved Path,” *ASME J. Mech. Des.*, **126**, pp. 667–672.
- [11] Howell, L. L., 2001, *Compliant Mechanisms*, Wiley, New York.